HHS Public Access

Author manuscript

Nat Struct Mol Biol. Author manuscript; available in PMC 2024 April 01.

Published in final edited form as:

Nat Struct Mol Biol. 2023 October ; 30(10): 1516–1524. doi:10.1038/s41594-023-01081-w.

Structure of the Preholoproteasome Reveals Late Steps in Proteasome Core Particle Biogenesis

Richard M. Walsh Jr.[1,2,*], **Shaun Rawson**[1,2,*], **Helena M. Schnell**[3], **Benjamin Velez**[3], **Tamayanthi Rajakumar**[3], **John Hanna**[3,#]

[1]Harvard Cryo-Electron Microscopy Center for Structural Biology, Harvard Medical School, Boston, Massachusetts, United States of America

[2]Department of Biological Chemistry and Molecular Pharmacology, Blavatnik Institute, Harvard Medical School, Boston, Massachusetts, United States of America

[3]Department of Pathology, Harvard Medical School and Brigham and Women's Hospital, Boston, Massachusetts, United States of America

Summary

Assembly of the proteasome's core particle, a barrel-shaped chamber of four stacked rings, requires 5 chaperones and 5 subunit propeptides. Fusion of two half-CP precursors yields a complete structure but remains immature until active site maturation. Using *S. cerevisiae*, we report a high-resolution cryo-EM structure of preholoproteasome, a post-fusion assembly intermediate. Our data reveal how CP midline-spanning interactions induce local changes in structure, facilitating maturation. Unexpectedly, we find that cleavage may not be sufficient for propeptide release, as residual interactions with chaperones like Ump1 hold them in place. We evaluated previous models proposing that dynamic conformational changes in chaperones drive CP fusion and autocatalytic activation by comparing preholoproteasome to pre-fusion intermediates. Instead, the data suggest a scaffolding role for the chaperones Ump1 and Pba1/Pba2. Our data clarify key aspects of CP assembly, suggest that undiscovered mechanisms exist to explain CP fusion/activation, and have relevance for diseases of defective CP biogenesis.

Introduction

The proteasome is a highly sophisticated protease that mediates the regulated degradation of misfolded or obsolete proteins, as well as regulatory proteins that control diverse cellular processes. Given its size and complexity, the proteasome cannot efficiently assemble spontaneously, but rather requires the assistance of dedicated chaperone proteins which are themselves excluded from mature proteasomes[1].

[#]Corresponding Author: jwhanna@bwh.harvard.edu.
[*]These authors contributed equally.

Author contributions

J.H., H.M.S., B.V., and T.R. performed the biochemical aspects of the work. R.W. and S.R. performed cryo-EM sample preparation, data collection, data processing, model building and refinement, and data analysis. R.W., S.R., and J.H. prepared the figures. J.H., R.W., and S.R. wrote the paper with input from all authors.

Declaration of Interests

The authors declare that they have no conflict of interest.

The proteasome's central core particle (CP) is a 700 kDa cylindrical chamber formed by four stacked heptameric rings. The outer α-rings contain a narrow gate that allows access of substrates to the CP interior. Each inner β-ring harbors three proteolytic active sites that cleave after hydrophobic (β5), basic (β2), and acidic residues (β1), respectively. The three active site subunits, along with two other non-enzymatic subunits (β6–7), are synthesized as precursor proteins with N-terminal propeptides of varying lengths. In addition to maintaining the active sites in an "off" state until the appropriate time, these propeptides also play important roles in CP assembly, in effect functioning as molecular chaperones[2,3]. Supporting this notion, the deleterious effects of removing these propeptides can be reverted by their expression in trans. The importance of the active site propeptides mirrors that of the active sites themselves (β5> β2> β1); in fact, deletion of β5's 75-residue propeptide is lethal[2,3]. In addition to these propeptides, there are five other chaperone proteins that function in CP assembly: Pba1-4 and Ump1[4–8]. An emerging family of human diseases is caused by defects in CP assembly. Inherited mutations in Ump1, Pba2, and portions of CP subunits that specifically function in CP assembly have been identified, leading to distinct but related diseases with both developmental defects and immune dysregulation[9–12].

CP assembly proceeds via an ordered pathway that begins with the generation of a complete α-ring in a process mediated by Pba1-4[1,12]. The Pba1/2 heterodimer binds on the outer surface of the α-ring, while Pba3/4 bind on the undersurface of the ring. β-subunits are then added sequentially, rather than en bloc. β2–4 are the first to enter, along with the fifth chaperone, Ump1. Ump1 binds β2's 29-residue propeptide, which in turn facilitates the incorporation of β3 and β4 through direct interactions[13]. Pba3/4 are released prior to the incorporation of these subunits, resulting in the 13S complex which was identified biochemically over 20 years ago and for which a high-resolution cryo-EM structure has been obtained recently[13]. β1, β5, and β6 join next, although it is unclear whether β1 precedes or follows β5/β6. The resulting complex is known as the 15S. A second high-resolution structure, the pre-15S, was obtained from a mutant that failed to incorporate β1[13]. Ump1 appeared to help position β5 and its propeptide in this structure. β7 is the last subunit to join, creating the half-CP[14–16]. Two of these then fuse to create the preholoproteasome, which contains all four rings but remains enzymatically inactive since the active site propeptides have not yet been cleaved. This autocatalytic activation is thought to be coupled to half-CP fusion, but the mechanistic details remain poorly understood. In the case of β1, there is evidence that contacts made by the opposing β7 subunit stabilize the active site catalytic triad (Thr20, Asp36, Lys52), thereby promoting autocatalytic activation[17]. Upon activation, Ump1 is degraded and Pba1/2 are released, resulting in mature 20S CP which can then associate with the regulatory particle (RP) which provides the ability to recognize and process substrates which have been marked for destruction by the small protein ubiquitin.

Structural analysis of CP assembly is hampered by the low abundance and transitory nature of CP assembly intermediates. The 13S and pre-15S structures were obtained from a previously generated mutant of β1 (*pre3-1*) that resulted in the specific accumulation of these intermediates[13,18]. Here we have extended that general approach by identifying another previously generated mutant, *pre1-1, 4-1*[18], that results in the accumulation of preholoproteasome through the joint impairment of β5 and β1 activation. We determined the structure of the preholoproteasome to a resolution of 3.0 Å. This structure reveals the

architecture and positions of Pba1/2, Ump1, and two of the active site propeptides at this late stage in assembly. Furthermore, by comparing this structure to earlier 13S and pre-15S assembly intermediates, we were able to follow the structure and conformation of the CP over a broad swath of the assembly pathway for the first time.

Results

Effects of the *pre1-1* and *pre4-1* Mutations

The *pre1-1*, *4-1* double mutant was first generated in the 1990's[18], but has not been extensively characterized and purified proteasomes harboring this double mutation have not been analyzed. In contrast, there has been prior analysis of each single mutant. The *pre1-1* mutation results in an S142F substitution in β4 and was previously shown to specifically impair the autocatalytic activation and overall activity of the β5 subunit, but not β2 or β1[2]. β4 directly contacts β5 from the opposite β-ring, a finding that was predicted more than twenty years ago based on biochemical and genetic assays[2], and then confirmed in the crystal structure of mature CP[19] (Fig. 1A–B). Ser-142 is present at the β4-β5 interface, and substitution with a bulky Phe residue is expected to disrupt this close interaction (Fig. 1B).

The *pre4-1* mutation results in deletion of the final 15 residues of β7[17]. β7 is the last subunit to join the half-CP, and is unique in having a long C-terminal extension that extends across the CP midline to sit in between the opposing β1 and β2 subunits (Fig. 1C). This C-terminal extension has been shown to participate both in half-CP fusion and β1's enzymatic activity through direct interaction with residues in β1 that support catalysis[17] (Fig. 1D). Thus, we hypothesized that the combined effect of the *pre1-1* and *pre4-1* mutations might specifically impair activation of the β5 and β1 active sites, resulting in a late block in CP maturation.

Purification and Analysis of CP from the *pre1-1, 4-1* Mutant

To affinity purify CP from the *pre1-1, 4-1* mutant, we inserted a C-terminal TEV-Protein A tag at the endogenous *PRE1* locus. High salt (500 mM NaCl) washes release RP, allowing for specific enrichment of CP particles. The electrophoretic profile of these CP was different from wild-type and suggested a strong defect in CP maturation, as evidenced by the accumulation of bands corresponding to the assembly chaperones Pba1/2 and the immature propeptide-bearing form of β5 (Fig. 2A), all three of which are excluded from mature CP. We next performed native gel electrophoresis followed by immunoblotting. We had previously developed an antibody against the β5 propeptide that specifically recognizes immature β5 with no reactivity against the mature, processed protein[13]. In the *pre1-1, 4-1* mutant, this antibody revealed a species running just above mature 20S, consistent with preholoproteasome (Fig. 2B). As expected, there was no immature β5 in the 20S species from either strain (Fig. 2B). We also observed an accumulation of sub-20S precursors (Fig. 2B). We analyzed the purified CP by size exclusion chromatography. Most of the material ran in the high molecular weight range, although there was a lower molecular weight shoulder, consistent with sub-20S species (Fig. 2C). Finally, we looked at the enzymatic activity of the purified material using fluorescent substrates that individually report on the proteasome's three different active sites (β5/chymotryptic, β2/tryptic, and β1/post-acidic). *pre1-1, 4-1* showed a near total loss of activity at the β5 and β1 active sites, whereas it

retained nearly wild-type activity at the β2 site (Fig. 2D). These results indicate that the *pre1-1, 4-1* mutations not only impair assembly, but also interfere with proteolytic activity of mature 20S particles, which make up a significant fraction of the purified material (Fig. 2B, left panel). Given that β5 is the most important of the three active sites, these results predict that the mutant should be strongly deficient in protein degradation in vivo. Indeed, we looked at two different short-lived proteasome substrates, the cytoplasmic protein Tmc1[20] and the ER-associated degradation (ERAD) substrate CPY*, and the degradation of both was markedly reduced in the *pre1-1, 4-1* strain (Fig. S1). Consistent with these results, there was strong compensatory upregulation of the proteasome biogenesis pathway mediated by the transcription factor Rpn4 (Fig. 2E). Since the proteasome is essential for viability, these results imply that *pre1-1, 4-1* cells survive largely due to preservation of β2 activity.

We analyzed the purified material from the *pre1-1, 4-1* mutant by cryo-EM. There was a complex mixture of species present (Fig. S2). The most abundant species by far was 20S CP (2.4 Å; Fig. S2–4), which is not surprising since the proteasome is essential for viability. Consistent with the biochemical data (Fig. 2B), we identified a subpopulation that appeared consistent with the preholoproteasome (Fig. 2F). These species were capped at either end of the CP by Pba1/2 and contained two copies of Ump1 within the CP barrel (Fig. 3A). Although this species represented less than 3% of the total particles, we were able to obtain an overall resolution of 3.0 Å, allowing for molecular modeling.

The β4-S142F mutation appeared to have a major impact on the opposing β5 subunit, which shows significantly lower local resolution compared to the rest of the preholoproteasome structure, likely reflecting subunit flexibility (Fig. S5). Interestingly, this region was well-resolved in the 20S proteasome (Fig. S5). Furthermore, the β5 catalytic triad appeared to be largely intact in the 20S CP, suggesting that the observed defects in β5 activity (Fig. 2D) may reflect dynamic aspects of the catalytic cycle that are not visualized in a single static structure.

Sub-20S particles were also identified (Fig. S2), consistent with the biochemical data (Fig. 2B–C). However, their resolutions were not in a range suitable for molecular modeling, and they were not studied further.

Structure and Contacts of Ump1

In the 13S and pre-15S structures, Ump1 is situated at the interface between the α- and the β-rings[13]. Its extended helical conformation allows it to wind around the CP contacting most of the CP subunits (α7, α1–4, β2–5) as well as exclusively immature aspects of the CP (β2-propeptide, β5-propeptide, and Pba1). An interaction with β1 was not evaluable in those prior structures since they lacked this subunit. However, in the preholoproteasome it is clear that Ump1, and particularly its helix #3, makes an extended multipoint interaction with β1 (Fig. 3B–C). This interaction involved the main body of β1. Whether Ump1 also contacts β1's propeptide, analogously to the β2 and β5 propeptides, remains unknown as most of the propeptide was not resolved (see below). Thus, Ump1 appears to also help recruit and position β1 within the nascent CP and, overall, contacts at least 5 of the 7 β-subunits (Fig. 3B).

Ump1 is required for half-CP fusion[4]. One model to explain this invokes a handshake-like mechanism where Ump1 extends across the CP midline to promote dimerization and fusion. The structure of the preholoproteasome shows how two Ump1 molecules are situated within the CP chamber (Fig. 3A), but provides little evidence to support this model as each Ump1 subunit was fully contained within its respective half of the CP (Fig. 3A), similar to its arrangement in the pre-fusion structures. The distance between the two Ump1 molecules is large (~40 Å). However, Ump1 residues 1–20 still remain unresolved, and so we cannot fully exclude this model. It has also been suggested that conformational changes in Ump1 may be important for driving fusion or other late events in CP assembly. We directly compared the position of Ump1 before and after CP fusion, and see little evidence of change in Ump1's overall structure or position within the CP (Fig. 3A).

Structure of the β2-Propeptide and its C-Terminal Extension

The 29-residue β2-propeptide runs across the interior surface of its neighboring subunit, β3, and then turns sharply at the β3/β4 junction to course towards the α-ring where it terminates in multiple contacts with Ump1[13]. In the preholoproteasome, the N-terminal 18 residues of the propeptide were well resolved and showed a position nearly identical to that seen in the 13S/pre-15S structures (Fig. 4A). In particular, the propeptide's N-terminus remained extensively bound to Ump1. The part of the propeptide more proximal to the active site (residues 19–29) was poorly resolved (Fig. 4A). This lack of resolvability could potentially reflect cleavage of the propeptide resulting in increased local flexibility, while preservation of intersubunit contacts at the propeptide's N-terminus prevents the propeptide from dissociating from the rest of β2.

In addition to its propeptide, β2 has a long C-terminal domain that wraps around β3 on the outer surface of the CP[17]. Most of the C-terminal domain (residues 221–240) was unresolved in the earlier pre-15S structure. In addition to β3 laterally, this region also interacts with the opposing β6 subunit at the CP midline[19]. In the preholoproteasome, the overall position of β3 was shifted toward β6 and the CP midline, indicating that the β3/β6 interaction, which is not present prior to half-CP fusion, is involved in helping β3 to assume its mature position. In turn, more of β2's C-terminal domain, and especially the β2 residues that interact with β3, were resolved in preholoproteasome (Fig. 4B; only residues 223–230 were missing). These findings demonstrate how CP fusion, and the resulting cross-midline contacts, play an important role in CP assembly.

A small segment of β1's 19-residue propeptide was resolved, extending directly out from the active site threonine-20 (residues 14-19; Fig. 4C). The overall trajectory of the propeptide was towards the interior of the CP and the resolved portion passed alongside its neighbor, β2. Due to the low local resolution, it is unclear whether the propeptide has been cleaved.

The β5 propeptide was not resolved, likely due to flexibility in β5 more generally, resulting from the destabilizing effects of the β4-S142F mutation. The structure does not inform the positions of the β6 and β7 propeptides as they were unresolved.

Analysis of the Pba1/2 Assembly Chaperones

Pba1/2 are present on the outer surface of the α-ring, and each protein inserts its C-terminal tail via a HbYX (hydrophobic-Tyr-any) motif into pockets at the α5/6 and α6/7 interfaces, respectively[21]. A surprising aspect of their function is that Pba1's N-terminus is inserted through the CP gate into the barrel's interior where it interacts with Ump1, the β5-propeptide, and all 7 α-subunits[13]. Pba1/2 achieve this feat by directly stimulating gate opening[22]. Prior work has suggested that conformational changes in Pba1/2 may occur during CP assembly. In particular, a low resolution structure (19 Å) of a pre-fusion intermediate suggested that Pba1/2 occupy a more central position over the α-ring prior to fusion[23]. This is in contrast to a crystal structure obtained by binding recombinant, bacterially expressed Pba1/2 to mature chemically inhibited yeast CP, where Pba1/2 were more eccentrically located at the α5–7 side of the ring[21]. We were able to address these discrepant results by comparing the position of Pba1/2 before and after fusion. In all three structures--13S, pre-15S, and preholoproteasome--Pba1/2 are in the eccentrically-located position described in the crystal structure (Fig. 5A). Furthermore, the precise positioning of Pba1/2 is remarkably consistent across the structures without any obvious conformational changes (Fig. 5B).

Discussion

We report here a high-resolution structure of a late CP assembly intermediate, the preholoproteasome. A previous structure of the preholoproteasome was obtained from the *pre1-1* single mutant; however, the low resolution (21 Å) precluded molecular modeling and neither Ump1 nor any of the propeptides were resolved[23]. Our structure provides detailed insight into the consequences of the *pre1-1, 4-1* mutations, explaining how these specific defects in the β4 and β7 subunits impact overall CP assembly. A broader question relates to how physiologically relevant this structure is to the authentic preholoproteasome assembly intermediate. Several lines of evidence suggest that our structure may be closely related to the authentic preholoproteasome. First, the overall structures and positions of Pba1/2, Ump1, and the β2-propeptide closely match those seen in two earlier stage structures, the 13S and pre-15S, obtained from an unrelated mutant[13]. In that *pre3-1* mutant, β1 fails to integrate during assembly; those structures therefore contain only wild-type subunits and, at least in the case of the 13S, precisely match its biochemically defined composition. Second, the positions of Ump1, Pba1/2, and the β2-propeptide are concordant with previously determined cross-linking data[23]. Third, the majority of species identified in this mutant were essentially mature 20S, suggesting that the mutations slow assembly but do not create an insurmountable obstacle to CP biogenesis.

This work identifies several important aspects of CP assembly. First, we identified extensive interactions between Ump1 and β1, indicating that Ump1 helps to position incoming β1 subunits within the nascent CP. This observation extends Ump1's overall reach to include 5 β-subunits (β1–5), 5 α-subunits (α7, α1–4), and Pba1, a remarkable feat for a natively unstructured 17 kDa protein. Recent biochemical work suggests that the very N-terminus of Ump1 interacts with the N-terminal propeptide of β7[24], neither of which were resolved in our structure. If so, this would add still another β-subunit to Ump1's repertoire. Second,

and unexpectedly, our results indicate that cleavage of a propeptide may not be sufficient to trigger its release, as residual interactions with chaperones like Ump1 can continue to hold them in place. Alternately, it could be that in wild-type cells additional cleavage events within the propeptide might allow for release from these interactions. These considerations raise interesting questions about the fate of the propeptides. If there is no mechanism to release them from Ump1, then it would seem most likely that they are degraded along with Ump1 at the end of assembly. Third, our results reveal how CP fusion can influence the final structure of the CP, as midline-spanning interactions can alter subunit conformations, as in the case of β2, β3, and β6.

Our results allow for the comparison of high-resolution structures which span a significant proportion of the assembly pathway (Fig. 6). Previous models of CP assembly have proposed that dynamic structural rearrangements may drive half-CP fusion, autocatalytic activation, and perhaps other aspects of the pathway. In one model, Ump1 is thought to prevent CP fusion until the appropriate moment, and release of this inhibitory checkpoint is mediated by a binding-induced conformational change in Ump1[14]. In the preholoproteasome, the overall position of Ump1 is essentially unchanged from that of the 13S/pre-15S despite CP fusion having occurred. We should note, however, that residues 1–20 of Ump1 were not resolved, and so such a model remains possible. A second intriguing model of CP fusion invokes a handshake-like mechanism whereby Ump1 would extend across the CP midline to recruit the opposing half-CP and stimulate fusion. Since Ump1 is found in both half-CP species, this model would also imply that dimerization of Ump1 at the CP midline drives fusion. Our data reveal the orientation of two Ump1 molecules in a CP intermediate and not only is there no midline-spanning Ump1 density, but the two Ump1 molecules appear to be quite far from each other. Pba1/2 have also been proposed to undergo dynamic rearrangements over the course of CP assembly[23]. Our data fail to support this model as the position and conformation of Pba1/2 are highly similar both before and after CP fusion. The overall impression to date from high-resolution structural analysis is one where the CP chaperones play more of a scaffolding or structural role in the assembly process, helping to ensure the proper incorporation and configuration of CP subunits. At present, this model is based mainly on structural analysis and so detailed functional testing of this model will be an important goal for future work.

In summary, our data provide a high-resolution structural basis for understanding and analyzing late steps in CP maturation, uncovering important conceptual aspects of the process. The lack of evidence for previously proposed dynamic models suggests that alternate, yet to be discovered, mechanisms likely exist to regulate half-CP fusion and autocatalytic activation. We expect that continued structural and functional analyses of this process will inform these and other aspects of CP assembly, as well as those diseases directly caused by defects in CP biogenesis.

Methods

Strains, Plasmids, and Antibodies

The *pre1-1, 4-1* mutant has been previously described[18]. To purify CP from this strain, we inserted a genomically integrated C-terminal Pre1-TEV-ProA tag, resulting in sJH998. The

strain was verified by PCR and immunoblot. Yeast were cultured at 30°C in YPD (1% yeast extract, 2% Bacto-peptone, and 2% dextrose).

The following antibodies and dilutions were used: anti-Alpha5[13] (1:2500), anti-β5-propeptide[13] (1:2500), anti-Rpn4[25] (1:2000), anti-Tmc1[20] (1:2000), anti-HA (Roche #12013819001) (1:1000), anti-Hog1 (Santa Cruz #165978 HRP) (1:2000).

The CPY*-HA plasmid, and the cycloheximide chase assay, have been described in detail[26].

CP Purification and Analysis

Proteasome was affinity purified using IgG resin (MP Biomedicals; ICN55961) and CP was isolated using high salt (500 mM NaCl) washes as previously described[13]. Purified proteasomes were analyzed by standard SDS-polyacrylamide gel electrophoresis (PAGE) followed by Coomassie staining or immunoblotting. Native gel analysis was performed using 3–8% Tris-Acetate gels (Invitrogen), followed by Coomassie staining or immunoblotting.

Cryo-EM Sample Preparation

Cryo-EM samples were prepared as previously described[13]. Affinity purified CP was further purified using size-exclusion chromatography in a buffer of 50 mM Tris, pH 7.5, 1 mM EDTA, and 100 mM NaCl. The CP-containing fractions were concentrated to ~2.4 mg/mL and supplemented with 0.5 μL of a 7.0 mM Fos-Choline, fluorinated solution (Anatrace) immediately prior to disposition onto 400 mesh Quantifoil Cu 1.2/1.3 grids which were glow discharged in a PELCO easiGLOW (Ted Pella) at 0.39 mBar, 15 mA for 30 s. Samples were vitrified using a Vitrobot Mark IV (Thermo Fisher Scientific), with a wait time of 15 s, blot time of 8 s, and a blot force of 20 at 100% humidity. All imaged samples were prepared during the same freezing session.

Cryo-EM Data Collection and Processing

Cryo-EM data were collected and processed as previously described[13]. Data were collected in two imaging sessions from two samples on a 300 kV Titan Krios G3i Microscope (Thermo Fisher Scientific) equipped with a K3 direct electron detector (Gatan) and a GIF quantum energy filter (25 eV; Gatan) using counted mode using the automated data collection software SerialEM[27] at the Harvard Cryo-Electron Microscopy Center for Structural Biology at Harvard Medical School. Details of the data collection and dataset parameters are summarized in Table 1. Dose-fractionated images were gain normalized, aligned, dose-weighted, and summed using MotionCor2[28]. Contrast transfer function (CTF) and defocus value estimation were performed using CTFFIND4[29]. Details of the data processing strategy are shown in Extended Data Fig. 2. Each dataset was processed independently for each session, before combination for the final refinements. In short, particle picking was carried out using crYOLO[30] followed by initial 2D classification within Relion[31] to give 2,868,028 particles. Heterogeneous classification in cryosparc[32] was used to sort particles into 20S containing species (20S alone, preholoproteasome (PHP), and Blm10-containing species), small sub-20S species, or into “junk” classes which identified 1,494,219 20S containing particles. 20S-containing species underwent Bayesian particle polishing

and CTF refinement within Relion, then further heterogeneous refinement in cryosparc to identify PHP and 20S populations. 20S particles were combined at this point and following a further heterogeneous refinement giving 766,100 total particles and non-uniform refinement in cryosparc produced a reconstruction at 2.4 Å with C2 symmetry imposed. PHP particles underwent further 3D classification in Relion using symmetry relaxation to produce 68,930 PHP species resulting in a 3.0 Å reconstruction following combination, subsequent CTF refinement, and non-uniform refinement within cryosparc with C2 symmetry imposed. Structural biology applications used in this project other than cryosparc were compiled and configured by SBGrid[33].

Model Building and Refinement

The *pre1-1,4-1* 20S model was built using 1RYP as a starting model, while the *pre1-1, 4-1* preholoproteasome used 7LS6 as a starting model. For both models, components were first rigid body fit into the cryo-EM density using UCSF Chimera[34]. This was followed by iterative cycles of manual building and refinement using Coot[35] and ISOLDE[36]for manual building, and Phenix[37] for real space refinement.

Data availability

Cryo-EM maps and atomic model coordinates have been deposited in the Electron Microscopy Data Bank and the Protein Data Bank, respectively: *pre1-1, 4-1* preholoproteasome (EMD-40838, PDB 8T08) and *pre1-1, 4-1* 20S proteasome (EMD-40944, PDB 8T0M). Additional PDB structures referenced here include 5CZ4, 7LSX, and 7LS6; additional EMD structures include 23508, 23503, 23502.

Supplementary Material

Refer to Web version on PubMed Central for supplementary material.

Acknowledgements

We thank Daniel Finley for assistance with size exclusion chromatography. This work was supported by NIH grant R01-GM144367 (to J.H. and R.W.).

References

1. Rousseau A & Bertolotti A Regulation of proteasome assembly and activity in health and disease. Nat Rev Mol Cell Biol 19, 697–712 (2018). [PubMed: 30065390]
2. Chen P & Hochstrasser M Autocatalytic subunit processing couples active site formation in the 20S proteasome to completion of assembly. Cell 86, 961–72 (1996). [PubMed: 8808631]
3. Jager S, Groll M, Huber R, Wolf DH & Heinemeyer W Proteasome beta-type subunits: unequal roles of propeptides in core particle maturation and a hierarchy of active site function. J Mol Biol 291, 997–1013 (1999). [PubMed: 10452902]
4. Ramos PC, Hockendorff J, Johnson ES, Varshavsky A & Dohmen RJ Ump1p is required for proper maturation of the 20S proteasome and becomes its substrate upon completion of the assembly. Cell 92, 489–99 (1998). [PubMed: 9491890]
5. Hirano Y et al. A heterodimeric complex that promotes the assembly of mammalian 20S proteasomes. Nature 437, 1381–5 (2005). [PubMed: 16251969]
6. Hirano Y et al. Cooperation of multiple chaperones required for the assembly of mammalian 20S proteasomes. Mol Cell 24, 977–84 (2006). [PubMed: 17189198]

7. Le Tallec B et al. 20S proteasome assembly is orchestrated by two distinct pairs of chaperones in yeast and in mammals. Mol Cell 27, 660–74 (2007). [PubMed: 17707236]
8. Kusmierczyk AR, Kunjappu MJ, Funakoshi M & Hochstrasser M A multimeric assembly factor controls the formation of alternative 20S proteasomes. Nat Struct Mol Biol 15, 237–44 (2008). [PubMed: 18278055]
9. Poli MC et al. Heterozygous Truncating Variants in POMP Escape Nonsense-Mediated Decay and Cause a Unique Immune Dysregulatory Syndrome. Am J Hum Genet 102, 1126–1142 (2018). [PubMed: 29805043]
10. de Jesus AA et al. Novel proteasome assembly chaperone mutations in PSMG2/PAC2 cause the autoinflammatory interferonopathy CANDLE/PRAAS4. J Allergy Clin Immunol 143, 1939–1943 e8 (2019). [PubMed: 30664889]
11. Watanabe A, Yashiroda H, Ishihara S, Lo M & Murata S The Molecular Mechanisms Governing the Assembly of the Immuno- and Thymoproteasomes in the Presence of Constitutive Proteasomes. Cells 11(2022).
12. Schnell HM, Walsh RM, Rawson S & Hanna J Chaperone-mediated assembly of the proteasome core particle - recent developments and structural insights. J Cell Sci 135(2022).
13. Schnell HM et al. Structures of chaperone-associated assembly intermediates reveal coordinated mechanisms of proteasome biogenesis. Nat Struct Mol Biol 28, 418–425 (2021). [PubMed: 33846632]
14. Li X, Kusmierczyk AR, Wong P, Emili A & Hochstrasser M beta-Subunit appendages promote 20S proteasome assembly by overcoming an Ump1-dependent checkpoint. EMBO J 26, 2339–49 (2007). [PubMed: 17431397]
15. Marques AJ, Glanemann C, Ramos PC & Dohmen RJ The C-terminal extension of the beta7 subunit and activator complexes stabilize nascent 20 S proteasomes and promote their maturation. J Biol Chem 282, 34869–76 (2007). [PubMed: 17911101]
16. Hirano Y et al. Dissecting beta-ring assembly pathway of the mammalian 20S proteasome. EMBO J 27, 2204–13 (2008). [PubMed: 18650933]
17. Ramos PC, Marques AJ, London MK & Dohmen RJ Role of C-terminal extensions of subunits beta2 and beta7 in assembly and activity of eukaryotic proteasomes. J Biol Chem 279, 14323–30 (2004). [PubMed: 14722099]
18. Gerlinger UM, Guckel R, Hoffmann M, Wolf DH & Hilt W Yeast cycloheximide-resistant crl mutants are proteasome mutants defective in protein degradation. Mol Biol Cell 8, 2487–99 (1997). [PubMed: 9398670]
19. Groll M et al. Structure of 20S proteasome from yeast at 2.4 A resolution. Nature 386, 463–71 (1997). [PubMed: 9087403]
20. Guerra-Moreno A & Hanna J TMC1 Is a Dynamically Regulated Effector of the RPN4 Proteotoxic Stress Response. J Biol Chem 291, 14788–95 (2016). [PubMed: 27226598]
21. Stadtmueller BM et al. Structure of a proteasome Pba1-Pba2 complex: implications for proteasome assembly, activation, and biological function. J Biol Chem 287, 37371–82 (2012). [PubMed: 22930756]
22. Schnell HM et al. Mechanism of proteasome gate modulation by assembly chaperones Pba1 and Pba2. J Biol Chem 298, 101906 (2022). [PubMed: 35398095]
23. Kock M et al. Proteasome assembly from 15S precursors involves major conformational changes and recycling of the Pba1-Pba2 chaperone. Nat Commun 6, 6123 (2015). [PubMed: 25609009]
24. Zimmermann J, Ramos PC & Dohmen RJ Interaction with the Assembly Chaperone Ump1 Promotes Incorporation of the beta7 Subunit into Half-Proteasome Precursor Complexes Driving Their Dimerization. Biomolecules 12(2022).
25. Guerra-Moreno A & Hanna J Induction of proteotoxic stress by the mycotoxin patulin. Toxicol Lett 276, 85–91 (2017). [PubMed: 28529145]
26. Weisshaar N, Welsch H, Guerra-Moreno A & Hanna J Phospholipase Lpl1 links lipid droplet function with quality control protein degradation. Mol Biol Cell 28, 716–25 (2017). [PubMed: 28100635]
27. Mastronarde DN Automated electron microscope tomography using robust prediction of specimen movements. J Struct Biol 152, 36–51 (2005). [PubMed: 16182563]

28. Zheng SQ et al. MotionCor2: anisotropic correction of beam-induced motion for improved cryo-electron microscopy. Nat Methods 14, 331–332 (2017). [PubMed: 28250466]
29. Rohou A & Grigorieff N CTFFIND4: Fast and accurate defocus estimation from electron micrographs. J Struct Biol 192, 216–21 (2015). [PubMed: 26278980]
30. Wagner T et al. SPHIRE-crYOLO is a fast and accurate fully automated particle picker for cryo-EM. Commun Biol 2, 218 (2019). [PubMed: 31240256]
31. Scheres SH RELION: implementation of a Bayesian approach to cryo-EM structure determination. J Struct Biol 180, 519–30 (2012). [PubMed: 23000701]
32. Punjani A, Rubinstein JL, Fleet DJ & Brubaker MA cryoSPARC: algorithms for rapid unsupervised cryo-EM structure determination. Nat Methods 14, 290–296 (2017). [PubMed: 28165473]
33. Morin A et al. Collaboration gets the most out of software. Elife 2, e01456 (2013). [PubMed: 24040512]
34. Pettersen EF et al. UCSF Chimera--a visualization system for exploratory research and analysis. J Comput Chem 25, 1605–12 (2004). [PubMed: 15264254]
35. Emsley P, Lohkamp B, Scott WG & Cowtan K Features and development of Coot. Acta Crystallogr D Biol Crystallogr 66, 486–501 (2010). [PubMed: 20383002]
36. Croll TI ISOLDE: a physically realistic environment for model building into low-resolution electron-density maps. Acta Crystallogr D Struct Biol 74, 519–530 (2018). [PubMed: 29872003]
37. Liebschner D et al. Macromolecular structure determination using X-rays, neutrons and electrons: recent developments in Phenix. Acta Crystallogr D Struct Biol 75, 861–877 (2019). [PubMed: 31588918]

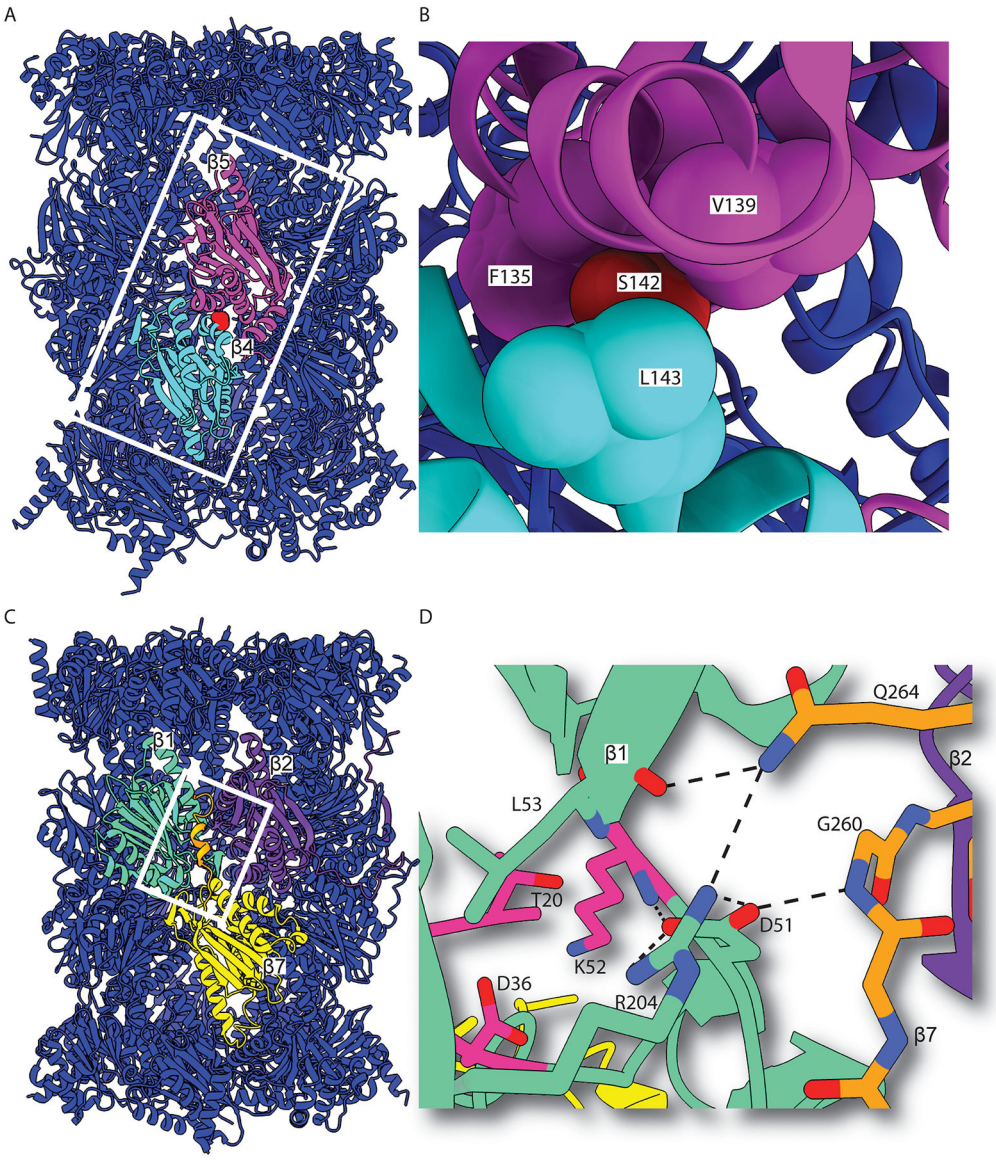

Fig. 1. Proposed consequences of the *pre1-1* and *pre4-1* mutations.

A) Structure of wild-type CP with the midline-spanning interaction between β4 and β5 highlighted. *Pre1-1* results in a β4-S142F mutation. The position of S142 is shown in red. B) Close-up view of β4-S142 which is present at the tightly packed interface between the two subunits. Bulky substitution at this site is predicted to disrupt the β4/β5 interface. C) Structure of wild-type CP showing how β7's C-terminal region extends across the midline to sit in between β1 and β2. D) β7's C-terminal region has been proposed to stimulate autocatalytic activation of β1 by stabilizing β1's catalytic triad (shown in pink), especially Lys52 (numbered as Lys33 in mature CP). Images prepared from PDB: 5CZ4. Dashed lines indicate hydrogen bonds.

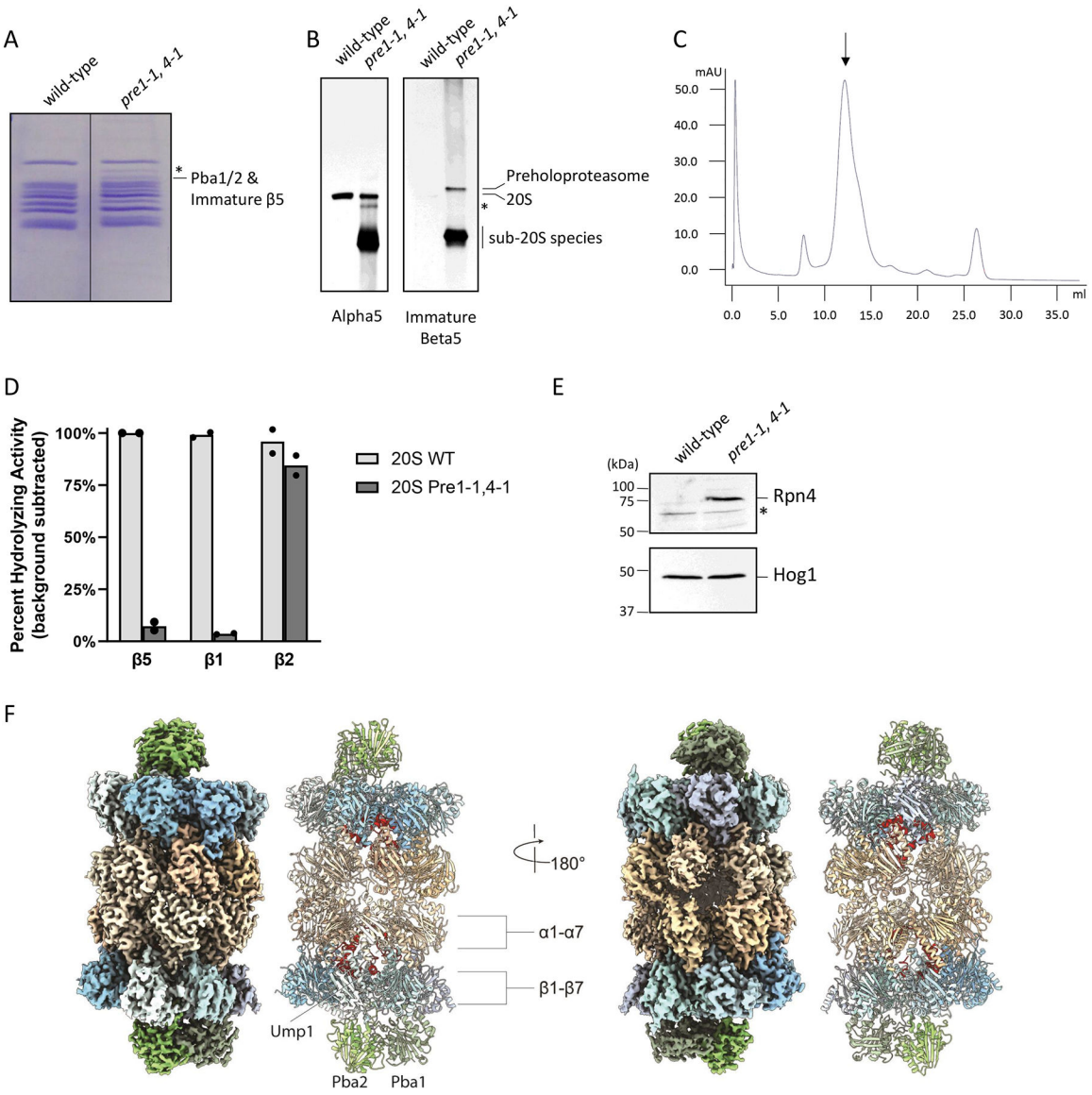

Fig. 2. Biochemical and Structural Analysis of *pre1-1, 4-1* Proteasomes.

A) Affinity purified material from wild-type and *pre1-1, 4-1* was analyzed by SDS-PAGE followed by Coomassie staining. Similar results were seen in 4 experiments. B) The same material was analyzed by native gel electrophoresis followed by immunoblotting with antibodies that recognize CP subunit α5 or immature β5. Note that the preholoproteasome species is of low abundance, and therefore not visualized with the anti-α5 antibody. Asterisk denotes a species in the *pre1-1, 4-1* mutant whose identity is unknown. Similar results were seen in 3 experiments. C) Size exclusion chromatography of the purified material from *pre1-1, 4-1*. Heavier material runs to the left. Arrow indicates the population selected for cryo-EM analysis. Similar results were seen in 2 experiments. mAU indicates the intensity of UV absorption. D). CP (15 nM) enzymatic activity was determined for each of the three active sites using the fluorogenic substrates suc-LLVY-AMC (β5), Z-LLE-AMC (β1), and Boc-LRR-AMC (β2). Data points from biologic duplicates are shown. Similar results were

seen in two experiments, each with duplicates. E) Upregulation of Rpn4-mediated new proteasome biogenesis in the *pre1-1, 4-1* mutant, as determined by immunoblot analysis of whole cell extracts. Upper panel, anti-Rpn4 antibody. Lower panel, anti-Hog1 antibody (loading control). Similar results were seen in four experiments. F) Cryo-EM structure of the preholoproteasome (3.0 Å) with its associated molecular model.

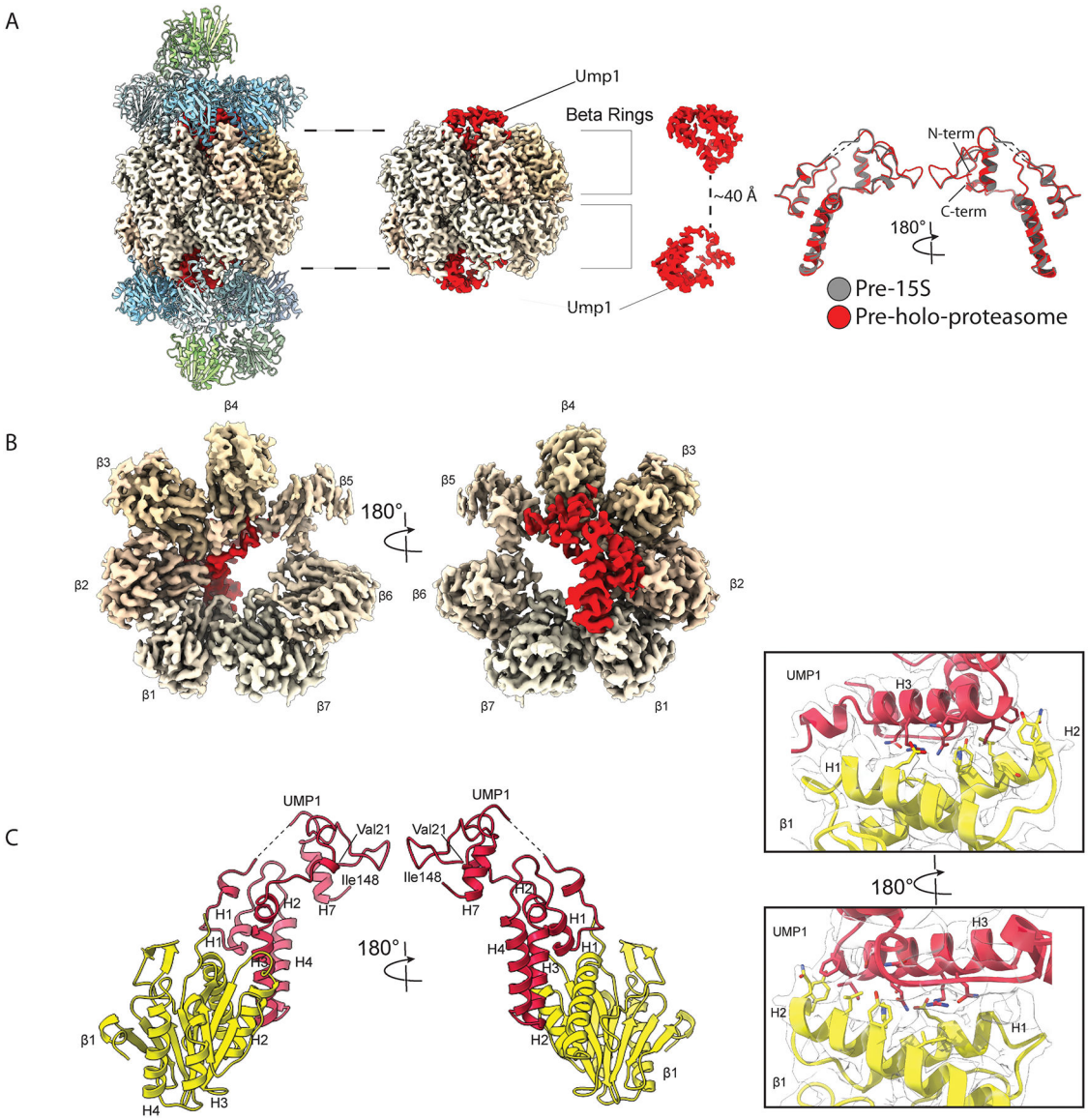

Fig. 3. Subunit Contacts and Overall Positioning of Ump1 within the Preholoproteasome.

A) Two Ump1 molecules are present within the preholoproteasome, although each appears to be contained within its respective half-CP with a large distance spanning the resolved densities (middle panel). Significant conformational changes in Ump1 before and after CP fusion were not detected (right panel). B) Ump1 spans most of the β-ring, making extensive contacts with β1-β5. C) Detailed contacts between Ump1 and β1, which were not detectable in the prior 13S and pre-15S structures, as these complexes lacked β1.

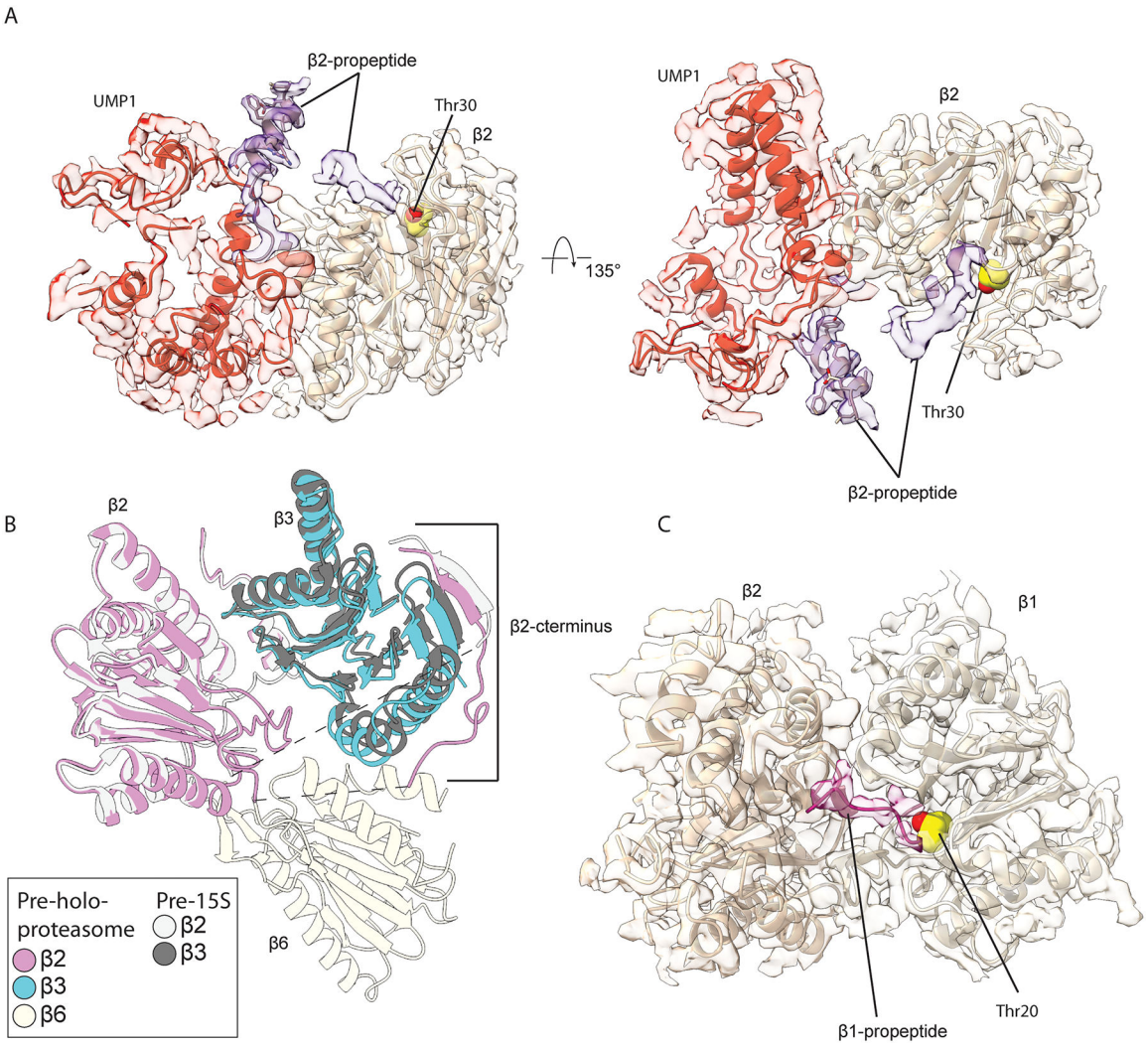

Fig. 4. The β2 propeptide and C-terminal Extension.

A) The N-terminal 18 residues of the β2 propeptide are well-resolved and remain extensively bound to Ump1. In contrast, the residues closer to the active site (19–29) are poorly resolved, likely reflecting flexibility in this region which in turn suggests that the propeptide has been cleaved. B) The position of β3 is shifted after CP fusion towards the midline through its contacts with the opposing β6 subunit. These contacts are further reflected in the increased resolution of β2's long C-terminal extension in the preholoproteasome relative to the pre-15S complex. C) A portion of the β1 propeptide (residues 14-19) was resolved in the preholoproteasome, extending directly from the active site Thr20, oriented towards the center of the CP, and passing nearby β2.

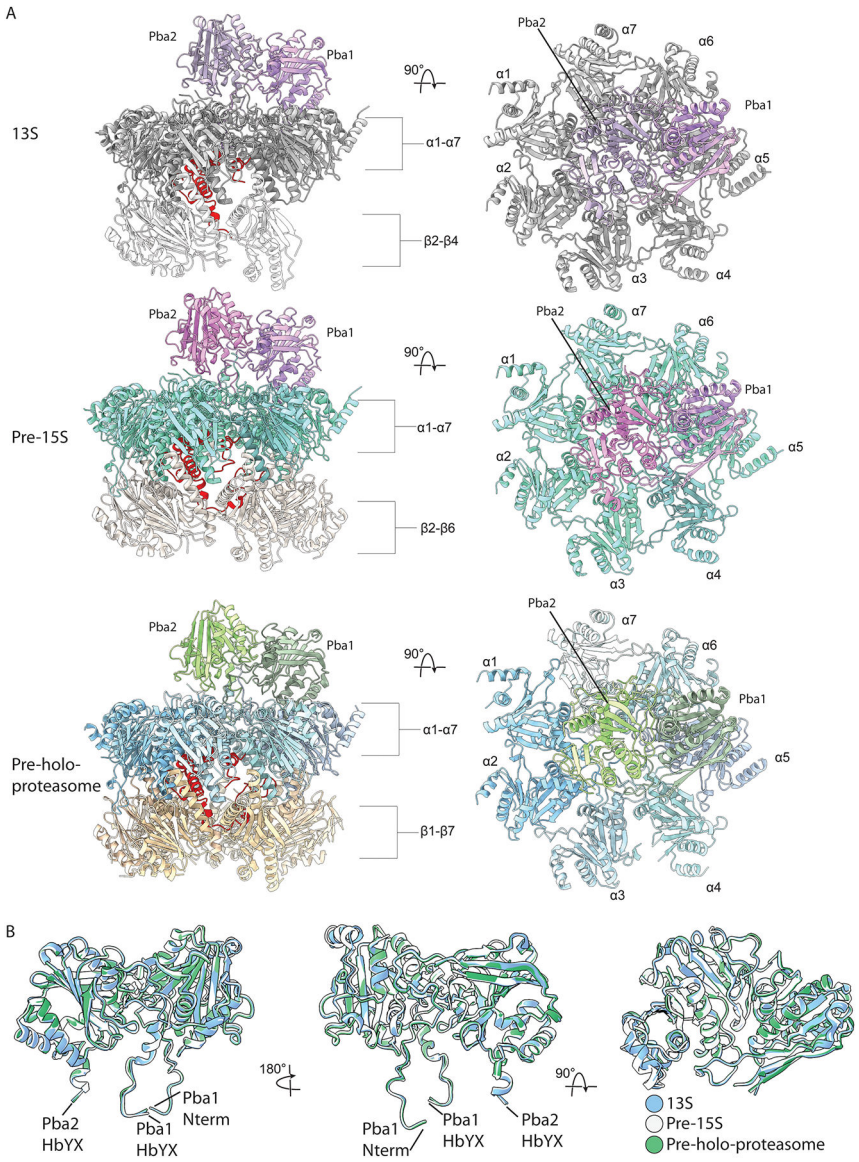

Fig. 5. Comparison of the Position and Conformation of Pba1/2 over the Course of CP Assembly.

A) The position of Pba1/2 on the α-ring is shown for 13S, pre-15S, and preholoproteasome assembly intermediates, and appears very similar throughout. B) Overlay of Pba1/2 from the three assembly intermediates shows little evidence of conformational changes during these stages of CP assembly.

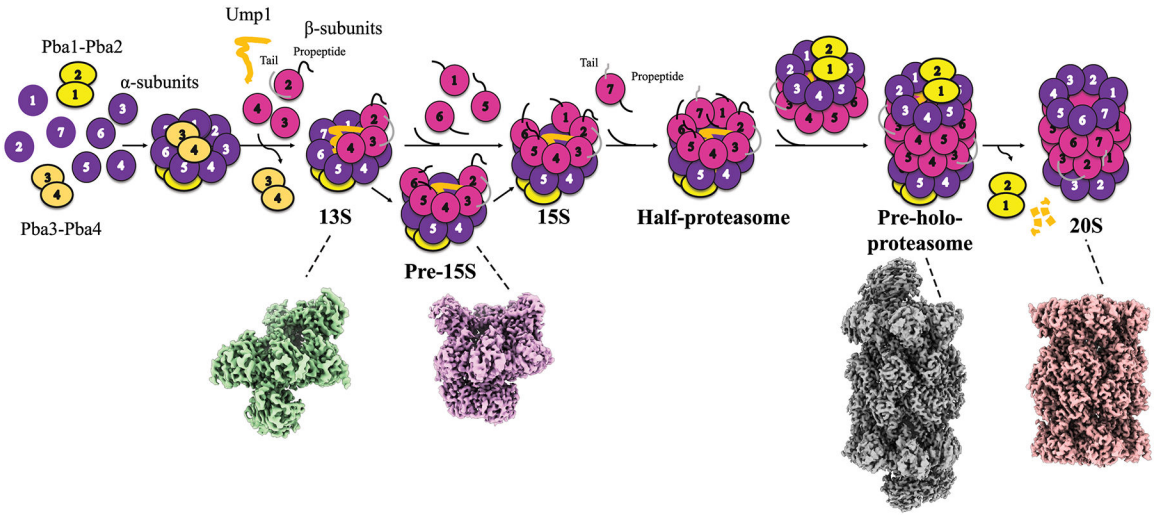

Fig. 6. Summary of High-Resolution Structural Analysis of CP Assembly.

Schematic representation of the known steps and assembly intermediates in CP biogenesis, coupled with their associated high-resolution structures identified here and in ref. 13. 13S, EMD-23508; pre-15S, EMD-23503; preholoproteasome (this work); and 20S, EMD-23502.

Table 1:

Cryo-EM data collection, refinement and validation statistics

	Pre-holo Proteasome (EMDB-40938, PDB 8T08)	Pre1-1/Pre4-1 20S (EMD-40944, PDB 8T0M)
Data collection and processing		
Magnification	47,169	
Voltage (kV)	300	
Electron exposure (e^{-}/Å^{-2})	55.6 (collection 1)	
	53.0 (collection 2)	
Defocus range (μm)	0.8, 2.2	
Pixel size (Å)	1.06	
Symmetry imposed	C2	C2
Initial particle images (no.)	2,868,028	
Final particle images (no.)	68,930	766,100
Map Resolution (Å)	3.0	2.4
FSC threshold	0.143	
Map resolution range (Å)		
Refinement		
Initial model used	7LS6	1RYP
Model resolution (Å)	3.30	2.50
FSC threshold	0.500	0.500
Map-sharpening B-factor (Å^2)	−79.8	−86.7
Model composition		
Non-hydrogen atoms	55,120	47,542
Protein residues	7,044	6,102
B factors (Å2)		
Protein	67.45	35.68
R.M.S.D. deviations		
Bond lengths (Å)	0.003	0.003
Bond angles (°)	0.472	0.564
Validation		
MolProbity score	1.28	1.34
Clashscore	5.29	5.34
Poor rotamers (%)	0.07	1.17
Ramachandran plot		
Favored (%)	98.22	98.57
Allowed (%)	1.78	1.43
Disallowed (%)	0.00	0.00